RSC Advances

ROYAL SOCIETY OF CHEMISTRY

www.rsc.org/advances

Cite this: DOI: 10.1039/c0xx00000x

www.rsc.org/xxxxxx

PAPER

Rational synthesis of novel π-conjugated poly(1,5-diaminoanthraquinone) for high-performance supercapacitors

Minqiang Sun,[a] Qianqiu Tang, Tao Zhang and Gengchao Wang*[a]

Received (in XXX, XXX) Xth XXXXXXXXX 200X, Accepted Xth XXXXXXXXX 200X

DOI: 10.1039/b000000x

Novel π-conjugated poly(1,5-diaminoanthraquinone) (PDAA) is successfully synthesized using $Ce(SO_4)_2$ with suitable redox potential through controlling polymerization temperature. The as-prepared PDAA under optimal condition displays homogeneous submicron particles, excellent π-conjugated structure as well as high conductivity (1.15×10^{-3} S cm^{-1}). Such unique features make the PDAA an ideal electrode material for electrochemical energy storage. As a supercapacitor electrode, the PDAA exhibits a high specific capacitance (406.3 F g^{-1}), desirable rate performance as well as superior cycle life (9.3% capacitance loss after 20000 cycles). This simple and cost-effective method without any external additives and stabilizers may provide valuable guidance for the rational preparation of other novel micro-nanostructure π-conjugated conducting polymers.

1 Introduction

Nowadays, with a fast-growing market for portable electronic devices and electric vehicles, the development of high energy storage systems has become a global concern. Supercapacitors have attracted great scientific and technological attention for energy storage devices due to their high specific power and long cycle life over lithium ion batteries.[1-5] However, supercapacitors suffer from unsatisfactory energy density. To improve their energy performance, considerable efforts have been devoted to the development of electrode materials, which are mainly π-conjugated conducting polymers (CPs) and transition-metal oxides based on faradic redox charge storage.[6-10] CPs, such as polyaniline (PANI), polypyrrole (PPy), polythiophene (PTh) and their derivatives, have been extensively explored due to their ease of synthesis, controllable electrical conductivity and high energy storage capacity.[11-14] Unfortunately, these conventional CPs exhibit poor cycling stability derived from the volumetric changes during the doping/dedoping process, which restricts their practical applications.[15-17] Considering the ever-increasing demands for high-efficiency supercapacitors in the modern society, there is an urgent need to develop new-generation CPs with high-performance.

Recently, a novel wholly aromatic polymer called poly(1,5-diaminoanthraquinone) (PDAA) has roused research interests.[18-21] Through the hybridization of polyaniline backbones with 1,4-benzoquinone moiety, PDAA possesses enhanced electroactivity[22-24] and broadened potential window[24] compared with PANI and PPy. Moreover, PDAA with "supramolecular" structure exhibits better cycling stability than other reported CPs due to strong π-π stacking interaction among anthracene rings and hydrogen bonds between N-H and C=O groups.[19,25,26] So the PDAA can be anticipated as a promising candidate for supercapacitor electrodes. Up to now, some efforts have been devoted to the synthesis of PDAAs.[22-25,27] For instance, Naoi *et al.* adopted electropolymerization method to prepare the PDAA film with excellent electrochemical performance but it is not amenable to large-quantity production.[26] And Li *et al.* successfully synthesized the PDAA nanoparticles by chemically oxidative polymerization.[22] However, due to the low polymerization degree and imperfect π-conjugated structure, the PDAAs by chemical methods exhibit lower conductivity, which is unfavourable for potential applications. So achieving chemically rational synthesis of high-performance PDAA is the paramount challenge.

To improve the physicochemical properties of CPs, the morphology and chain structure should be controlled.[28-30] For chemically oxidative polymerization, the redox potential (RP) of oxidants and polymerization temperature are two key factors, which is largely in control of the performances of CPs.[31-32] Li *et al.* found that the oxidants with various RPs significantly affect the polymerization yield and macromolecular structure of PDAAs.[22] So the matching of RP between the oxidant and monomer is greatly key for the polymerization of CPs. Furthermore, it is known that the polymerization temperature can dominate the microstructure of CPs. However, the optimal oxidant for DAA monomer and perfect reaction temperature have not been achieved up to now, resulting in an unsatisfactory performance of PDAA.

Herein, we firstly report a simple strategy to synthesize novel π-conjugated PDAA with high performances through optimizing the RP of oxidant and controlling polymerization temperature. And a novel oxidant of $Ce(SO_4)_2$ with suitable redox potential was developed to prepare submicron-scale PDAA particles. Besides, the formation mechanism for PDAA particles under different temperatures was revealed. The as-prepared PDAA

using $Ce(SO_4)_2$ under appropriate temperature of 20°C delivers excellent conductivity (1.15×10^{-3} S cm^{-1}, markedly higher than previous reported PDAAs) as well as high specific capacitance of 406.3 F g^{-1}. More importantly, the prototype cell supercapacitor based on two symmetrical PDAA electrodes exhibits outstanding cycle life with only 9.3% capacitance loss after 20000 cycles, which is significantly superior to other reported CPs.

2 Experimental

2.1 Synthesis of poly(1,5-diaminoanthraquinone)

The poly(1,5-diaminoanthraquinone) (PDAA) was synthesized using an chemically oxidative polymerization method. Typical procedure was as follows: 5 mmol diaminoanthraquinone monomer (DAA) was dissolved in 200 mL 1 M H_2SO_4 DMAc solution, and then the mixture was poured into glass flask and stirred vigorously for half an hour. Meanwhile, the oxidant solution was prepared by dissolving $Ce(SO_4)_2$ (10 mmol) into 100 mL 1 M H_2SO_4 DMAc solution under sonication for 1 h. Then, the $Ce(SO_4)_2$ solution was added into the above DAA solution by dropwise at the rate of 1 drop per 3 s, and the reaction was carried out under stirring for 48 h at various polymerization temperatures (0, 20, 40 and 60°C). The mole reaction concentration of DAA (C_{DAA}) was controlled by 0.017 M. Finally, the resulting precipitates were filtered and washed with DMAc, ethanol and excess distilled water for several times to remove the remaining monomer, oxidant and oligomers. For comparison, the PDAAs with various oxidants were synthesized through the similar procedure above. In order to avoid misunderstanding, it is stated that the mentioned PDAA-X refers to the PDAA prepared with the oxidant of $Ce(SO_4)_2$ at X°C. The synthesis conditions and yields of PDAA with various oxidants and polymerization temperatures were listed in Table S1 and Table S2, respectively.

2.2 Characterization

The Fourier transform infrared spectroscopy (FTIR) spectra were recorded at a Nicolet 5700 spectrometer from KBr pellets. The UV-Vis spectra were obtained using a Shimadzu UV-2102PC spectrophotometer. X-ray diffraction (XRD) patterns were obtained by using a Rigaku D/Max 2550 VB/PC X-ray diffractometer with Cu Kα radiation. The morphologies of the samples were characterized by the field-emission scanning electron microscopy (FE-SEM, Hitachi S-4800) with an energy dispersive spectrometer (EDS, QUANTAX 400-30) and the transmission electron microscope (TEM, JEOL JEM-1400, 100 kV). X-ray photoelectron spectroscopy (XPS) analysis was performed in a thermo scientific ESCALAB 250Xi X-ray photoelectron spectrometer equipped with amonochromatic Al Kα X-ray source (1486.6 eV). The specific surface area (SSA) was measured on Molecular Devices SpectraMax M2 using the methylene blue adsorption method (ESI†). The conductivity of the samples was determined by PC40B digital resistance tester.

2.3 Electrochemical measurements

The working electrodes were prepared by mixing and grinding 75 wt.% of active material, 20 wt.% of acetylene black and 5 wt.% of poly(tetrafluoroethylene) (PTFE) binder in deionized water/ethanol mixed solution (1/9, v/v) to form a homogeneous slurry. The slurry was rolled and then pressed onto the titanium mesh. The mass of active material was about 2 mg. The prototype cell supercapacitors were composed of two symmetrical working electrodes sandwiched by a polypropylene (PP) separator in 1 M aqueous H_2SO_4 electrolyte.

Cyclic voltammetry (CV), galvanostatic charge/discharge and electrochemical impedance spectroscopy (EIS) were carried out in 1 M H_2SO_4 using a three-electrode mode on a CHI 660D electrochemical workstation. Platinum foil and Ag/AgCl electrode were used as counter electrode and reference electrode, respectively. The potential range for CV and charge/discharge tests was 0.2-0.9 V. The Nyquist diagrams were ran in the frequency range from 10^5 to 10^{-2} Hz with 5 mV amplitude. Cycling stability was performed by galvanostatic charge/discharge test with a program testing system (LAND CT2001A) using prototype cell supercapacitors.

The specific capacitance (*Cs*) of the electrode material could be calculated according to the following equation:

$$Cs = C/m = I/m(dV/dt)$$

where *Cs* is the specific capacitance, *I* is the discharge current, *m* is the mass of active electrode material and dV/dt denotes the slope of discharge curve (*V*-*t*).

3 Results and discussion

To select the optimum oxidant, the polymerization of DAA monomer was attempted with $(NH_4)_2S_2O_8$ (RP=2.05 V), H_2O_2 (1.77 V), $KMnO_4$ (1.51 V), $Ce(SO_4)_2$ (1.44 V), CrO_3 (1.35 V) and $FeCl_3$ (0.77 V) under the same conditions. As shown in Fig. 1a, the color of the solution with $(NH_4)_2S_2O_8$, H_2O_2 and $FeCl_3$ as oxidants is similar to that of DAA monomer while the resultant solution using $KMnO_4$, $Ce(SO_4)_2$ and CrO_3 turns brown or black, which indicates that too high or too low RP values are unfavorable for the polymerization of DAA. This is probably related to the coexistence of the oxidizable NH_2 and reducible C=O groups in DAA monomer. Furthermore, the highest polymerization yield (25.5%) is obtained by the oxidant of $Ce(SO_4)_2$ used (Table S1†).

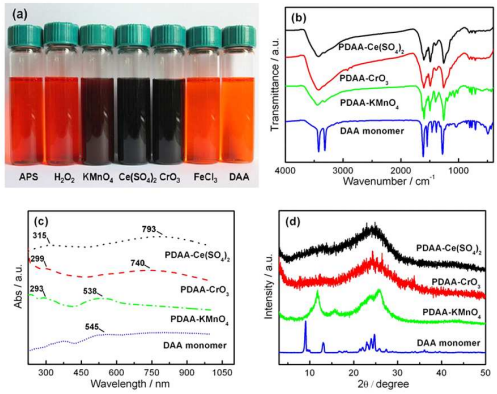

Fig. 1 (a) Photograph showing ethanol dispersions of raw DAA and PDAAs prepared with various oxidants at 20°C. (b) FTIR spectra, (c) UV-Vis spectra and (d) XRD patterns of DAA monomer and PDAAs prepared with various oxidants: $Ce(SO_4)_2$, CrO_3 and $KMnO_4$.

FTIR spectra of the PDAAs using $KMnO_4$, $Ce(SO_4)_2$ and CrO_3 all exhibit the main bands at 1605, 1493 and 1259 cm^{-1} corresponding to the C=C stretching vibrations of N=Q=N and N-Q-N rings and the C-N stretching vibration, respectively, which is

completely distinguished from DAA monomer (Fig. 1b). This indicates that π-conjugated polymers are synthesized by $KMnO_4$, $Ce(SO_4)_2$ and CrO_3. For PDAA-$KMnO_4$, there still exist some extra bands similar to DAA monomer, suggesting the formation of oligomers along with PDAA polymers, thereby leading to the brown color of polymerization solution (Fig. 1a).

As seen from UV-Vis spectra, the PDAA-$KMnO_4$ presents similar bands compared with DAA monomer, which further indicates that there exist some DAA oligomers in PDAA-$KMnO_4$. However, both PDAA-$Ce(SO_4)_2$ and PDAA-CrO_3 display two obvious bands at *ca* 290-320 and 700-800 nm, corresponding to π-π* transition in quinonediimine-like units and polaron transition in polyaniline-like units, respectively,[22,33] further verifying the formation of π-conjugated polymers (Fig. 1c). Moreover, the band of polaron transition of PDAA-$Ce(SO_4)_2$ red-shifts compared with that of PDAA-CrO_3 (from 740 nm to 793 nm). This indicates higher π-conjugated degree of the PDAA-$Ce(SO_4)_2$. The XRD patterns of the three PDAAs all display a broad diffraction peak at about 2θ=25°, which implies the amorphous structure rather than highly crystalline structure of DAA monomer (Fig. 1d). In addition, an exceptional sharp peak at approximately 11.7° appears in PDAA-$KMnO_4$ pattern, which may be associated with DAA oligomer.

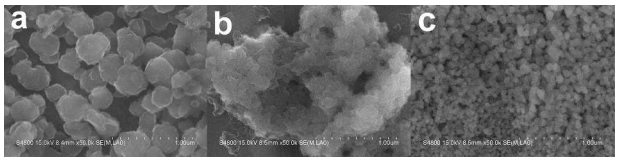

Fig. 2 FE-SEM images of PDAAs prepared with various oxidants: (a) $Ce(SO_4)_2$, (b) CrO_3 and (c) $KMnO_4$.

Interestingly, the oxidants with different RPs can make an enormous difference to the morphology of PDAAs (Fig. 2). PDAA-$Ce(SO_4)_2$ displays homogeneous submicron particles with the diameter of 200-300 nm while 100 nm nanoparticles for PDAA-$KMnO_4$. However, the PDAA-CrO_3 shows aggregated morphology.

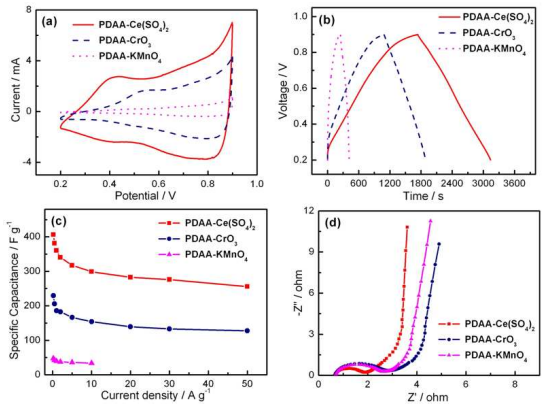

Fig. 3 The electrochemical performances of the PDAAs with various oxidants: $Ce(SO_4)_2$, CrO_3 and $KMnO_4$. (a) CV curves at a scan rate of 10 mV s^{-1}. (b) Galvanostatic charge/discharge curves at a current density of 0.2 A g^{-1}. (c) The specific capacitance as a function of various current densities. (d) Nyquist plots in the frequency range of 10^5-10^{-2} Hz.

Due to excellent π-conjugated structure for electron conduction and homogeneous submicron size, the conductivity of PDAA-$Ce(SO_4)_2$ reaches up to 1.15×10^{-3} S cm^{-1} (Table S1†). It is three orders of magnitude higher than that of PDAA-CrO_3 and PDAA-$KMnO_4$ as well as markedly superior to the prepared PDAAs by Li *et al.*[22]

The electrochemical performance of the PDAAs with various oxidants is shown in Fig. 3. The CV curves display two pairs of redox peaks at *ca* 0.4-0.5 and 0.8 V for PDAA-$Ce(SO_4)_2$ and PDAA-CrO_3 (Fig. 3a), corresponding to the transitions of quinine/hydroquinone (Q/HQ) and emelardine/quinine diimine, respectively,[23,25] which indicates good pseudocapacitive behavior for PDAAs. By contrast, the PDAA-$KMnO_4$ exhibits no obvious redox peak and a much smaller curve area. The charge/discharge curves of PDAAs exhibit symmetrical and mirror-like images, indicating the redox reaction of PDAAs is reversible (Fig. 3b).

And the specific capacitance of PDAA-$Ce(SO_4)_2$ is as high as 406.3 F g^{-1} at 0.2 A g^{-1}. Moreover, it retains about 63% capacitance with the growth of current density from 0.2 to 50 A g^{-1} while only 55.7% retention for PDAA-CrO_3 and even lower for PDAA-$KMnO_4$, which implies that PDAA-$Ce(SO_4)_2$ exhibits superior rate capability (Fig. 3c).

Generally, EIS is a powerful tool to understand the fundamental behaviors of electrode materials, as displayed in Fig. 3d. In high frequency region, the semicircle corresponds to the charge transfer resistance (R_{CT}) at the electrode/electrolyte interface. It is found that PDAA-$Ce(SO_4)_2$ exhibits the smallest R_{CT} (1.25 Ω), indicating its excellent ability of charge conduction. Besides, PDAA-$Ce(SO_4)_2$ shows a more nearly vertical line in low frequency region, revealing the ideal capacitive behavior. As a summary, $Ce(SO_4)_2$ is elected as the most appropriate oxidant to prepare high-performance PDAA, which is of great potential and value as a novel supercapacitor electrode.

Polymerization temperature is another vital factor to control the structure and morphology of CPs. So the influence of the temperature on the chemical structure, morphology and electrochemical performance for PDAA-$Ce(SO_4)_2$ is systematically investigated. As seen in Fig. 4a, three PDAAs at higher temperatures (≥20°C) exhibit similar FTIR absorption bands. The intensity of bands for N=Q=N ring at *ca* 1605 cm^{-1} strengthens as the temperature increases, which indicates high degree of oxidation for the PDAAs under higher temperatures. However, a strong and wide band at around 1130 cm^{-1} derived from the $Ce(SO_4)_2$ is displayed in PDAA-0 (Fig. 4a and Fig. S1a†). Besides, the UV-Vis spectrum of PDAA-0 (Fig. 4b) presents a strong band at 345 nm and a shoulder band at 556 nm similar to DAA monomer (Fig. 1c), suggesting the existence of DAA oligomers for PDAA-0. Thus it can be inferred that the complex of $Ce(SO_4)_2$ and DAA oligomer is formed at low temperature (0°C). But at higher polymerization temperatures (≥20°C), the as-prepared PDAAs display two obvious absorption bands at *ca* 290-320 and 600-800 nm similar to polyaniline. This indicates that low temperature is unfavorable for the formation of π-conjugated PDAAs. Furthermore, a red-shift of the band for polaron transition from 688 to 793 nm is observed as the temperature decreases from 60 to 20°C, which implies the highest π-conjugated degree for PDAA-20.

To investigate the chemical component and structure of PDAA, X-ray photoelectron spectroscopy (XPS) is employed. It can be seen from Fig. 4c that PDAA-20 displays primary C 1s, N 1s and

O 1s peaks. However, except for the above peaks, unique Ce 3d peaks at 880-930 eV are observed in PDAA-0 similar to $Ce(SO_4)_2$. And approximately 27 wt.% of Ce element is observed from the XPS, which is consistent with the EDS result of PDAA-0 (Fig. S2a†). Besides, the EDS mapping image shows that red bright dots are X-ray radial signals radiated from Ce element, which is homogenously distributed in PDAA-0 (Fig. S2b†). The detailed analysis of Ce 3d spectrum reveals the presence of two sets of spin-orbital multiplets (v and u), corresponding to the $3d_{3/2}$ and $3d_{5/2}$ core holes (Fig. S1b†).[34] Moreover, Ce 3d peaks of PDAA-0 shift to lower binding energy compared with $Ce(SO_4)_2$, which may be ascribed to the complexation between DAA oligomer and $Ce(SO_4)_2$ at 0°C. As shown in Fig. 4d, the signals of N 1s for PDAA-20 are fitted with peaks of quinonoid imine (=N–, 398.9 eV), benzenoid amine (–NH–, 399.5 eV) and protonated N^+ (400.7 eV), which further verifies that PDAA-20 is π-conjugated polymer like polyaniline. And for the N 1s spectrum of PDAA-0, an extra perdominant peak centered at 400.1 eV is observed due to the complexation of $–NH_2\cdots Ce$. This is in good accordance with our FTIR and UV-Vis results above.

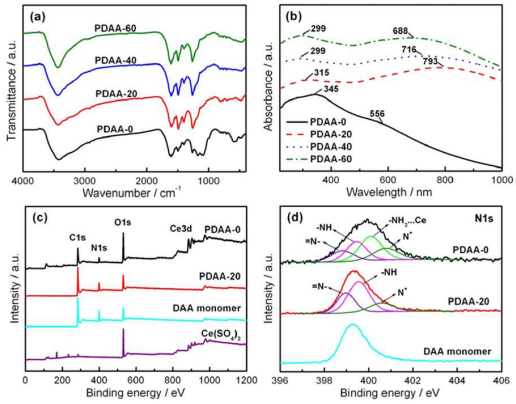

Fig. 4 (a) FTIR spectra and (b) UV-Vis spectra of PDAA-$Ce(SO_4)_2$ with various polymerization temperature, XPS spectra for (c) survey scan and (d) N 1s region of PDAA-0, PDAA-20, DAA monomer and $Ce(SO_4)_2$.

Fig. 5a-d presents the FE-SEM images of PDAA-$Ce(SO_4)_2$ under various polymerization temperatures. At low temperature of 0°C, PDAA-0 exhibits the aggregated structure consisting of numerous nanoparticles of 80-120 nm (Fig. 5a). Interestingly, the morphology occurs distinct change when the temperature rises to 20°C. As seen in Fig. 5b, the PDAA-20 displays homogeneous submicron particles with the diameter of 200-300 nm, which is further verified by TEM images (Fig. 5e-f). The image with higher magnification clearly reveals the internal structure of single PDAA particle like an "snowball". Based on DAA oligomers as central nucleation sites, the PDAA initial nanoparticles gradually grow similar to the "snowball rolling" process, which well confirms the self-nucleation of PDAAs. However, at higher polymerization temperature (40 or 60°C), the aggregated morphology is formed again, which is composed of 100-200 nm submicron particles (Fig. 5c-d).

Based on above analysis, the possible formation mechanism of PDAAs is illustrated in scheme 1. At low temperature (0°C), the complexation reaction between $Ce(SO_4)_2$ and DAA oligomer dominates due to the slow initiation rate of $Ce(SO_4)_2$, and the resultant complex further aggregates through π-π interaction and hydrogen bonds. As the polymerization temperature increases to 20°C, the initiation rate and chain propagation rate are moderate. So DAA oligomers with proper concentration are generated, acting as the active self-nucleation sites for the growth of PDAA-20, which is well proved by TEM image (Fig. 5f). Moreover, submicron-scale PDAA-20 particles can stay self-stable rather than conglomerated, which is ascribed to the static repulsion between negative charges of PDAA-20 ($C\text{-}O^-$, Zeta potential: -17.1 mV).[24] However, at higher temperatures (40 or 60°C), a large number of PDAA initial nanoparticles are generated, ascribed to fast initiation and propagation rate. Furthermore, due to high temperature and dense concentration of nanoparticles, brownian motion is accelerated, which makes the PDAA nanoparticles prefer to aggregate beyond the static repulsion.

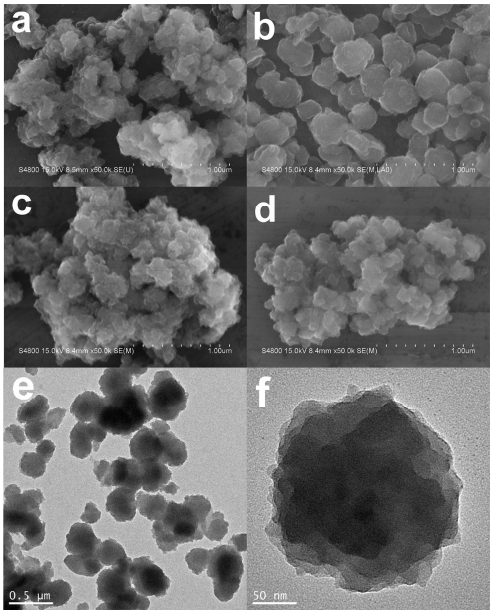

Fig. 5 FE-SEM images of (a) PDAA-0, (b) PDAA-20, (c) PDAA-40 and (d) PDAA-60 using the oxidant of $Ce(SO_4)_2$, (e, f) TEM images of PDAA-20 with low and high magnifications.

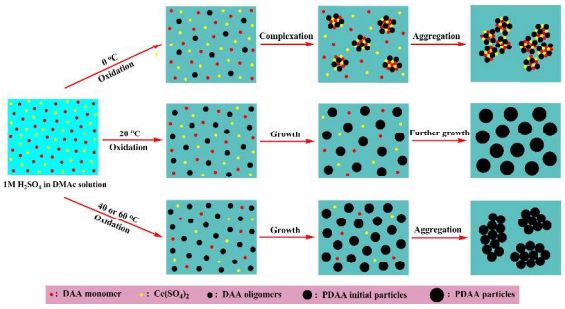

Scheme. 1 Schematic illustration for the formation of PDAA-$Ce(SO_4)_2$ with various polymerization temperatures.

Fig. 6 presents the electrochemical performance of PDAAs with various polymerization temperatures. At higher temperatures (≥20°C), the PDAAs exhibit similar CV and charge/discharge curves except for PDAA-0 (Fig. 6a-b). Due to the complex of $Ce(SO_4)_2$ and DAA oligomer formed at 0°C, PDAA-0 shows no obvious redox peak compared with three other PDAAs. Besides, PDAA-0 also displays a much smaller CV curve area and shorter discharge duration, indicating low specific capacitance.

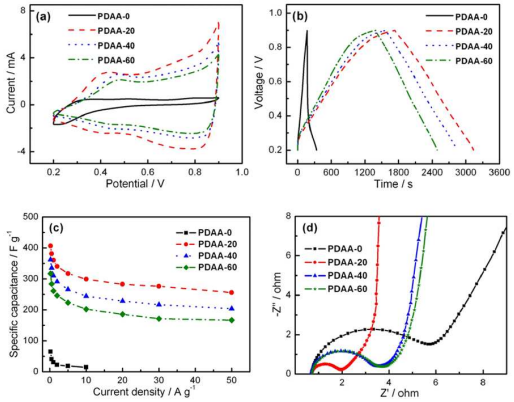

Fig. 6 The electrochemical performances of PDAA-$Ce(SO_4)_2$ with various polymerization temperatures. (a) CV curves at a scan rate of 10 mV s^{-1}. (b) Galvanostatic charge/discharge curves at a current density of 0.2 A g^{-1}. (c) The specific capacitance as a function of various current densities (d) Nyquist plots in the frequency range of 10^5-10^{-2} Hz.

Furthermore, PDAA-0 shows poor rate capability, which is ascribed to inferior conductivity of the complex. Conversely, at higher temperatures (≥20°C), the PDAAs exhibit excellent rate capability due to higher conductivity (Table S2†). And PDAA-20 possesses optimal 63% retention of initial specific capacitance (406.3 F g^{-1}) as the current density increases from 0.2 to 50 A g^{-1} (Fig. 6c), which is superior to other reported CPs.

It is found from Nyquist plots (Fig. 6d) that PDAA-0 exhibits the biggest R_{CT} and quite inclined curve in low frequency. However, under higher temperatures (≥20°C), the R_{CT} of PDAAs obviously decreases and the nearly vertical line is displayed. And the smallest R_{CT} is observed for PDAA-20. The performance difference of above PDAAs is mainly ascribed to their chemical structure, π-conjugated degree, morphology as well as specific surface area. The PDAA-20 possesses the highest π-conjugated degree, homogeneous submicron particles and the highest specific surface area (SSA) of 86.3 m^2 g^{-1}. As the polymerization temperature rises, PDAAs display aggregated morphology and the SSA gradually decreases (Table S2†). For the PDAA-0, though it possesses higher SSA of 71.8 m^2 g^{-1} due to numerous oligomer nanoparticles, PDAA-0 has very low polymerization degree and π-conjugated degree, which results in inferior electrochemical performance. Therefore, based on above analysis, the PDAA-20 is verified to possess optimal intriguing electrochemical performances.

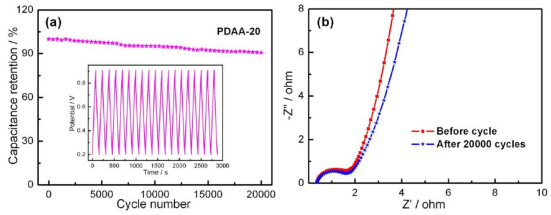

Fig. 7 (a) Cycling stability of prototype supercapacitor based on PDAA-20 at a current density of 1 A g^{-1}. The data were obtained from the two-electrode supercapacitor measured using galvanostatic charge/discharge technique, as seen from the inset. (b) Nyquist plots of the prototype supercapacitor based on PDAA-20 in the frequency range of 10^5-10^{-2} Hz before and after 20000 cycles.

More importantly, the prototype supercapacitor based on PDAA-20 possesses outstanding cycling stability with only 9.3% capacitance loss over 20000 cycles (Fig. 7a), which is significantly superior to other previous reported CPs.[16,17,33,35] The exceptional cycle life can be ascribed to less mechanical degradation by isotropic lattice expansion and shrinkage of peculiar π-stacked "supramolecule".[19,25,26] Furthermore, the stable intermediate "charge-transfer" complex between aniline moiety and benzoquinone molecule through the hydrogen bonds can largely enhance the chemical stabilization and prevent the migration of the benzoquinone, which is also beneficial to electrochemical cycling stability.[26]

In order to verify the cycling stability, EIS test was conducted before and after 20000 cycles (Fig. 7b). It is apparent that PDAA-20 maintains the same R_{CT} and displays only little inclined tendency for the line in low frequency region after cycles, revealing excellent ability of charge conduction. In addition, the FE-SEM images show no obvious change for the microstructure of PDAA-20 electrode wafer, as seen from Fig. S3†. So the above analysis further supports the conclusion of superior cycling stability for PDAA-20.

4 Conclusions

In summary, a facile and scalable strategy has been developed to prepare the submicron-scale PDAA particles using novel oxidant of $Ce(SO_4)_2$. The optimization of PDAAs is carried out through selecting RP of oxidant and controlling polymerization temperature. The formation mechanism of PDAAs indicates that the complex of $Ce(SO_4)_2$ and DAA oligomer is formed at 0°C, but real π-conjugated polymer obtained at higher temperature (≥20°C). Moreover, the as-prepared PDAA-20 possesses high specific capacitance of 406.3 F g^{-1}, desirable rate performance and superior cycling stability (90.7% capacitance retention after 20000 cycles). The intriguing supercapacitive performance is attributed to excellent π-conjugated degree, homogeneous submicron size and unique π-stacked supramolecular structure of PDAAs. In addition, the simple synthesis technique without any external additives and stabilizers is readily scalable to industrial levels. Therefore, this rational design may provide valuable guidance for the productive preparation of other π-conjugated CPs with novel micro-nano structure, and which can be commendably applied in energy storage devices, lithium ion batteries, chemical sensors, catalyst supports and so on.

Acknowledgments

We greatly appreciate the financial supports of National Natural Science Foundation of China (51173042), Shanghai Municipal Science and Technology Commission (12nm0504102), Fundamental Research Funds for the Central Universities, Innovation Program of Shanghai Municipal Education Commission (11ZZ55).

Notes and references

[a] *Key Laboratory for Ultrafine Materials of Ministry of Education, Shanghai Key Laboratory of Advanced Polymeric Materials, School of Materials Science and Engineering, East China University of Science & Technology, Shanghai 200237, China. E-mail: gengchaow@ecust.edu.cn*

† Electronic Supplementary Information (ESI) available: Experimental details and supplementary figures. See DOI: 10.1039/b000000x/

1 X. W. Yang, C. Cheng, Y. F. Wang, L. Qiu and D. Li, *Science*, 2013, **341**, 534.
2 H. Jiang, P. S. Lee and C. Z. Li, *Energy Environ. Sci.*, 2013, **6**, 41.
3 Y. Zhai, Y. Dou, D. Zhao, P. F. Fulvio, R. T. Mayes and S. Dai, *Adv. Mater.*, 2011, **23**, 4828.
4 S. W. Lee, B. M. Gallant, H. R. Byon, P. T. Hammond and Y. Shao-Horn, *Energy Environ. Sci.*, 2011, **4**, 1972.
5 P. Simon and Y. Gogotsi, *Nat. Mater.*, 2008, **7**, 845.
6 H. P. Cong, X. C. Ren, P. Wang and S. H. Yu, *Energy Environ. Sci.*, 2013, **6**, 1185.
7 X. Zhao, L. L. Zhang, S. Murali, M. D. Stoller, Q. H. Zhang, Y. W. Zhu and R. S. Ruoff, *ACS Nano*, 2012, **6**, 5404.
8 W. F. Wei, X. W. Cui, W. X. Chen and D. G. Ivey, *Chem. Soc. Rev.*, 2011, **40**, 1697.
9 H. L. Wang, H. S. Casalongue, Y. Y. Liang and H. J. Dai, *J. Am. Chem. Soc.*, 2010, **132**, 7472.
10 Q. Wu, Y. X. Xu, Z. Y. Yao, A. R. Liu and G. Q. Shi, *ACS Nano*, 2010, **4**, 1963.
11 D. Li, J. X. Huang and R. B. Kaner, *Acc. Chem. Res.*, 2009, **42**, 135.
12 B. K. Kuila, B. Nandan, M. Bohme, A. Janke and M. Stamm, *Chem. Commun.*, 2009, **38**, 5749.
13 L. Y. Yuan, X. Xiao, T. P. Ding, J. W. Zhong, X. H. Zhang, Y. H. Huang, J. Zhou and Z. L. Wang, *Angew. Chem. Int. Ed.*, 2012, **51**, 4934.
14 G. R. Li, Z. P. Feng, J. H. Zhong, Z. L. Wang and Y. X. Tong, *Macromolecules*, 2010, **43**, 2178.
15 K. Zhang, L. L. Zhang, X. S. Zhao and J. S. Wu, *Chem. Mater.*, 2010, **22**, 1392.
16 R. B. Ambade, S. B. Ambade, N. K. Shrestha, Y. C. Nah, S. H. Han, W. Lee and S. H. Lee, *Chem. Commun.*, 2013, **49**, 2308.
17 L. L. Zhang, S. Y. Zhao, X. N. Tian and X. S. Zhao, *Langmuir*, 2010, **26**, 17624.
18 Y. S. Zhao, J. S. Wu and J. X. Huang, *J. Am. Chem. Soc.*, 2009, **131**, 3158.
19 S. A. Hashmi, S. Suematsu and K. Naoi, *J. Power Sources*, 2004, **137**, 145.
20 V. Noël and H. N. Randriamahazaka, *Electrochem. Commun.*, 2012, **19**, 32.
21 Z. Algharaibeh and P. G. Pickup, *Electrochim. Acta*, 2013, **93**, 87.
22 X. G. Li, H. Li and M. R. Huang, *Chem. Eur. J.*, 2007, **13**, 8884.
23 S. Suematsu and K. Naoi, *J. Power Sources*, 2001, **97-98**, 816.
24 K. Naoi, S. Suematsu and A. Manago, *J. Electrochem. Soc.*, 2000, **147**, 420.
25 M. M. Gao, F. L. Yang, X. H. Wang, G. Q. Zhang, L. F. Liu, *J. Phys. Chem. C*, 2007, **111**, 17268.
26 K. Naoi, S. Suematsu, M. Hanada and H. Takenouchi, *J. Electrochem. Soc.*, 2002, **149**, A472.
27 M. M. Gao, F. L. Yang, G. Q. Zhang, L. F. Liu and X. H. Wang, *Electrochim. Acta*, 2009, **54**, 2224.
28 Y. Wang, H. D. Tran, L. Liao, X. F. Duan and R. B. Kaner, *J. Am. Chem. Soc.*, 2010, **132**, 10365.
29 N. Nuraje, K. Su, N. Yang and H. Matsui, *ACS Nano*, 2008, **2**, 502.
30 K. Wang, J. Y. Huang and Z. X. Wei, *J. Phys. Chem. C*, 2010, **114**, 8062.
31 H. J. Ding, M. X. Wan and Y. Wei, *Adv. Mater.*, 2007, **19**, 465.
32 G. C. Li, L. Jiang and H. R. Peng, *Macromolecules*, 2007, **40**, 7890.
33 J. J. Xu, K. Wang, S. Z. Zu, B. H. Han and Z. X. Wei, *ACS Nano*, 2010, **4**, 5019.
34 E. Beche, P. Charvin, D. Perarnau, S. Abanades and G. Flamant, *Surf. Interface Anal.*, 2008, **40**, 264.
35 M. Q. Xue, F. W. Li, J. Zhu, H. Song, M. N. Zhang and T. B. Cao, *Adv. Funct. Mater.*, 2012, **22**, 1284.

Table of contents

Colour graphic

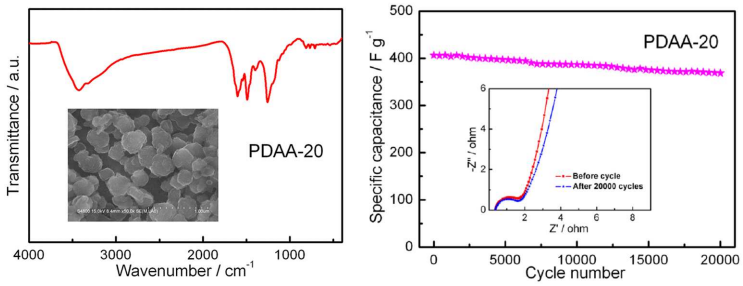

Text

A novel π-conjugated poly(1,5-diaminoanthraquinone) with high performance was developed through optimizing redox potential of oxidant and controlling polymerization temperature.